Supplemental Document

Optics EXPRESS

Tolerance to aberration and misalignment in a two-point-resolving image inversion interferometer: supplement

DAVID J. SCHODT,[1,2,*] PATRICK J. CUTLER,[2] FRANCISCO E. BECERRA,[1,3] AND KEITH A. LIDKE[1]

[1] *Department of Physics and Astronomy, University of New Mexico, Albuquerque, New Mexico, USA*
[2] *Teledyne Scientific & Imaging, LLC, USA*
[3] *Center for Quantum Information and Control, University of New Mexico, Albuquerque, New Mexico, USA*
[*] *david.schodt@teledyne.com*

Supplement DOI: https://doi.org/10.6084/m9.figshare.22665886

Parent Article DOI: https://doi.org/10.1364/OE.487808

Tolerance to Aberration and Misalignment in a Two-Point-Resolving Image Inversion Interferometer: supplemental document

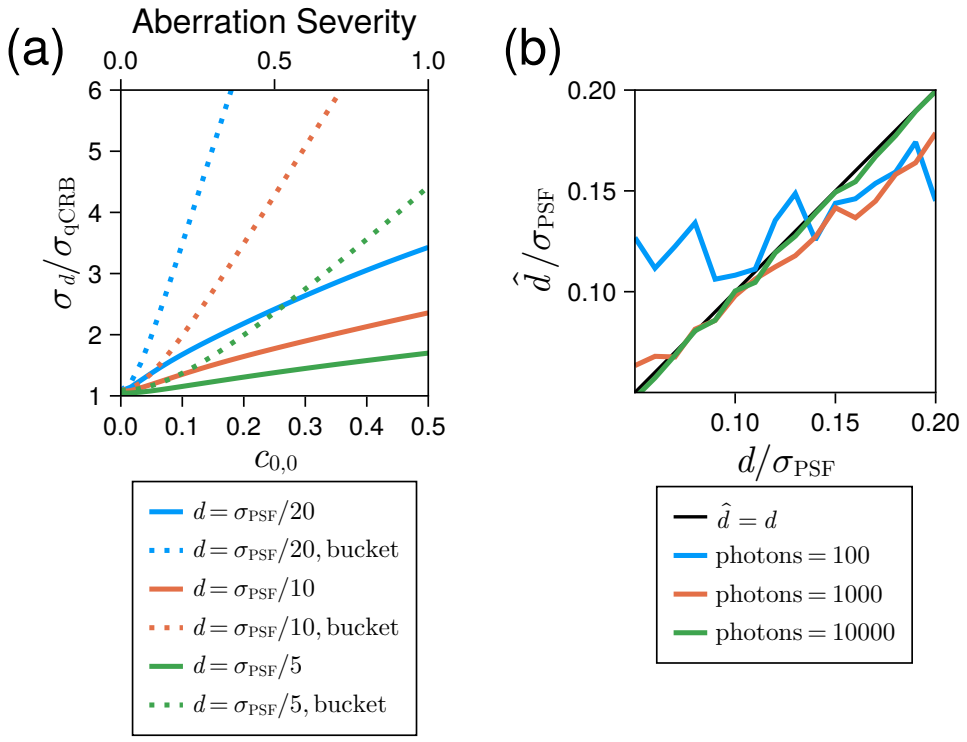

Fig. S1. Intra-SLIVER phase piston. (a) $\sigma_d/\sigma_{\mathrm{qCRB}}$ as a function of increasing piston (n=0, l=0) in one arm of the interferometer for pixelated (solid lines) and bucket (dashed lines) SLIVER measurements. (b) MLE of the separation for a Zernike coefficient of 0.25 at varying signal levels when the model has complete knowledge of the aberration.

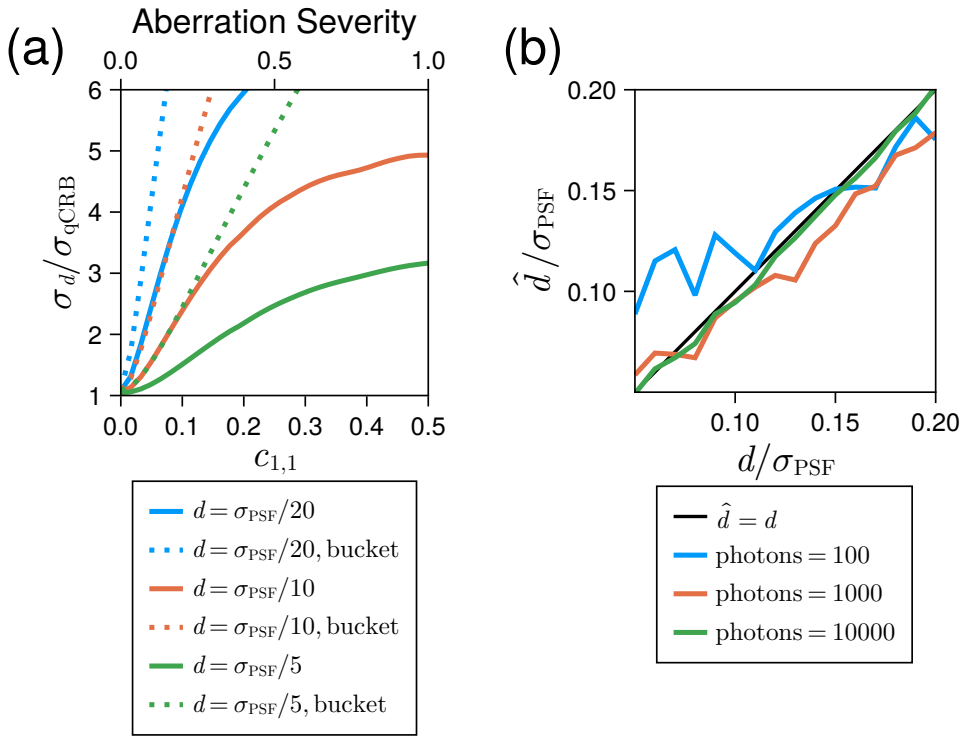

Fig. S2. Intra-SLIVER phase tilt. (a) $\sigma_d/\sigma_{\mathrm{qCRB}}$ as a function of increasing horizontal tilt (n=1, l=1) in one arm of the interferometer for pixelated (solid lines) and bucket (dashed lines) SLIVER measurements. (b) MLE of the separation for a Zernike coefficient of 0.25 at varying signal levels when the model has complete knowledge of the aberration.

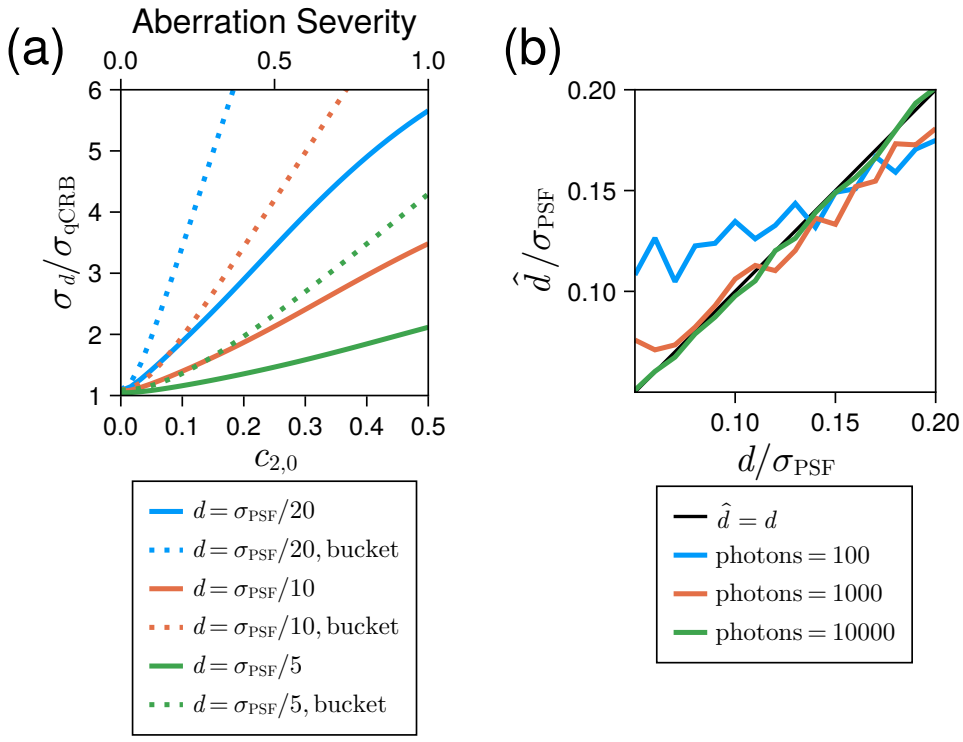

Fig. S3. Intra-SLIVER phase defocus. (a) $\sigma_d/\sigma_{\mathrm{qCRB}}$ as a function of increasing defocus (n=2, l=0) in one arm of the interferometer for pixelated (solid lines) and bucket (dashed lines) SLIVER measurements. (b) MLE of the separation for a Zernike coefficient of 0.25 at varying signal levels when the model has complete knowledge of the aberration.

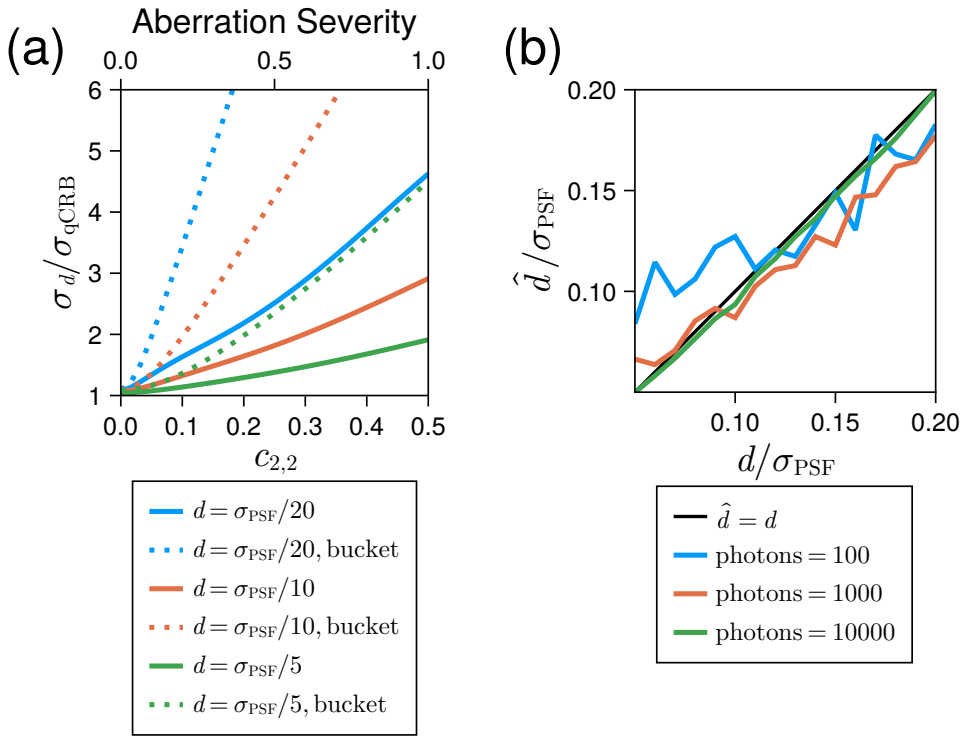

Fig. S4. Intra-SLIVER phase astigmatism. (a) $\sigma_d/\sigma_{\mathrm{qCRB}}$ as a function of increasing vertical astigmatism (n=2, l=2) in one arm of the interferometer for pixelated (solid lines) and bucket (dashed lines) SLIVER measurements. (b) MLE of the separation for a Zernike coefficient of 0.25 at varying signal levels when the model has complete knowledge of the aberration.

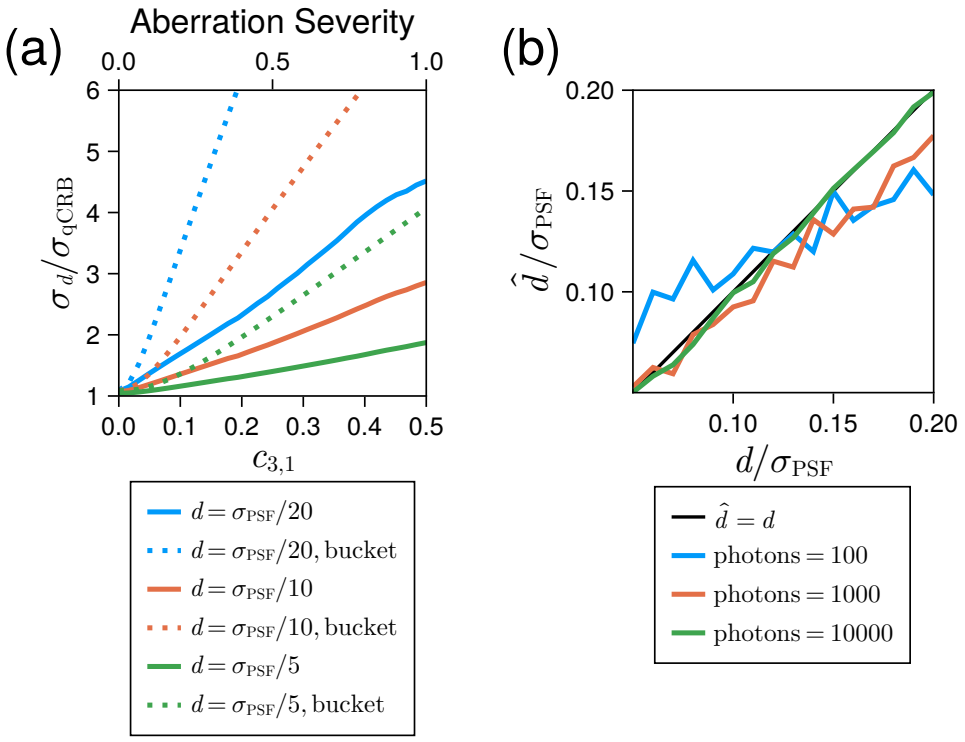

Fig. S5. Intra-SLIVER phase coma. (a) $\sigma_d/\sigma_{\mathrm{qCRB}}$ as a function of increasing horizontal coma (n=3, l=1) (i.e., coma along the axis of separation) in one arm of the interferometer for pixelated (solid lines) and bucket (dashed lines) SLIVER measurements. (b) MLE of the separation for a Zernike coefficient of 0.25 at varying signal levels when the model has complete knowledge of the aberration.

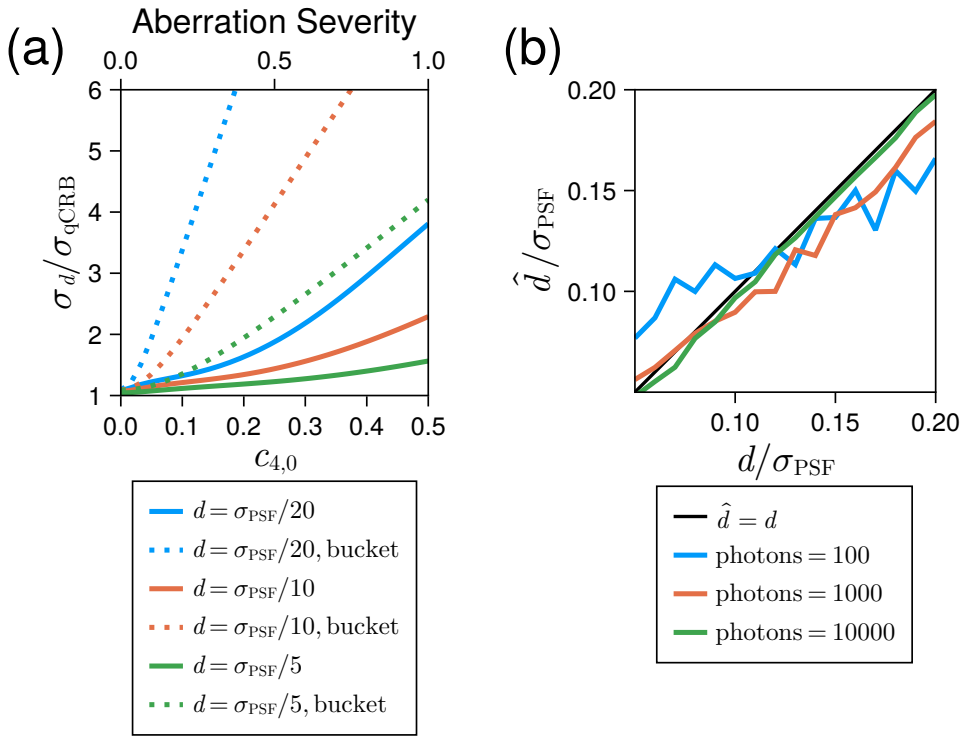

Fig. S6. Intra-SLIVER spherical aberration. (a) $\sigma_d/\sigma_{\mathrm{qCRB}}$ as a function of increasing spherical aberration (n=4, l=0) in one arm of the interferometer for pixelated (solid lines) and bucket (dashed lines) SLIVER measurements. (b) MLE of the separation for a Zernike coefficient of 0.25 at varying signal levels when the model has complete knowledge of the aberration.

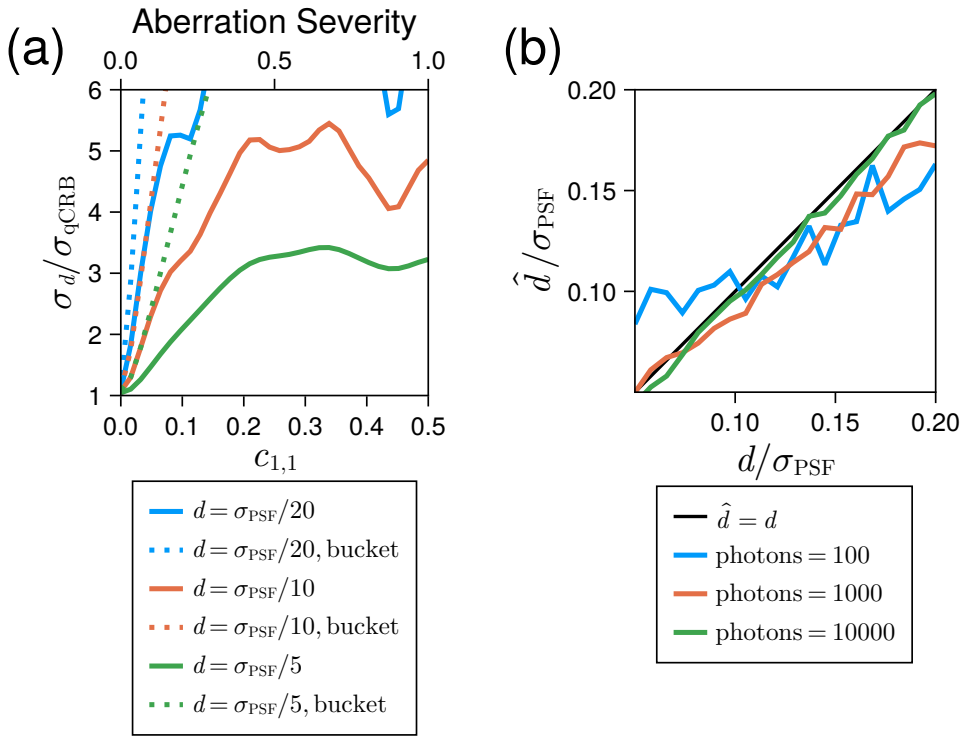

Fig. S7. Extra-SLIVER phase tilt. (a) $\sigma_d/\sigma_{\mathrm{qCRB}}$ as a function of increasing horizontal tilt (n=1, l=1) at the interferometer entrance for pixelated (solid lines) and bucket (dashed lines) SLIVER measurements. (b) MLE of the separation for a Zernike coefficient of 0.25 at varying signal levels when the model has complete knowledge of the aberration.

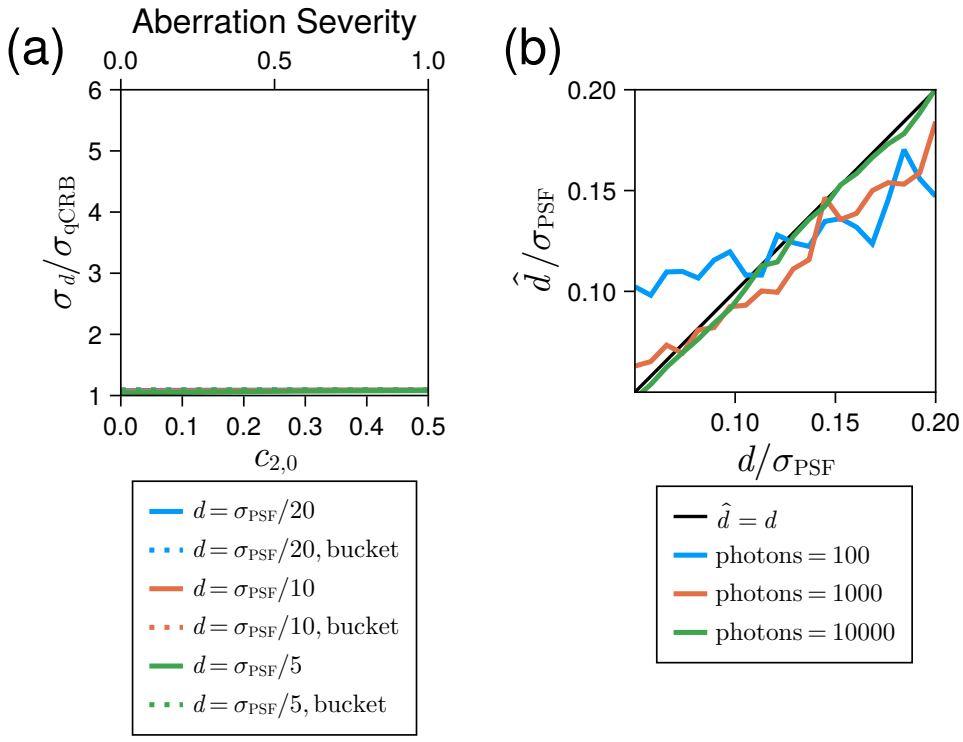

Fig. S8. Extra-SLIVER phase defocus. (a) $\sigma_d/\sigma_{\mathrm{qCRB}}$ as a function of increasing defocus (n=2, l=0) at the interferometer entrance for pixelated (solid lines) and bucket (dashed lines) SLIVER measurements. (b) MLE of the separation for a Zernike coefficient of 0.25 at varying signal levels when the model has complete knowledge of the aberration.

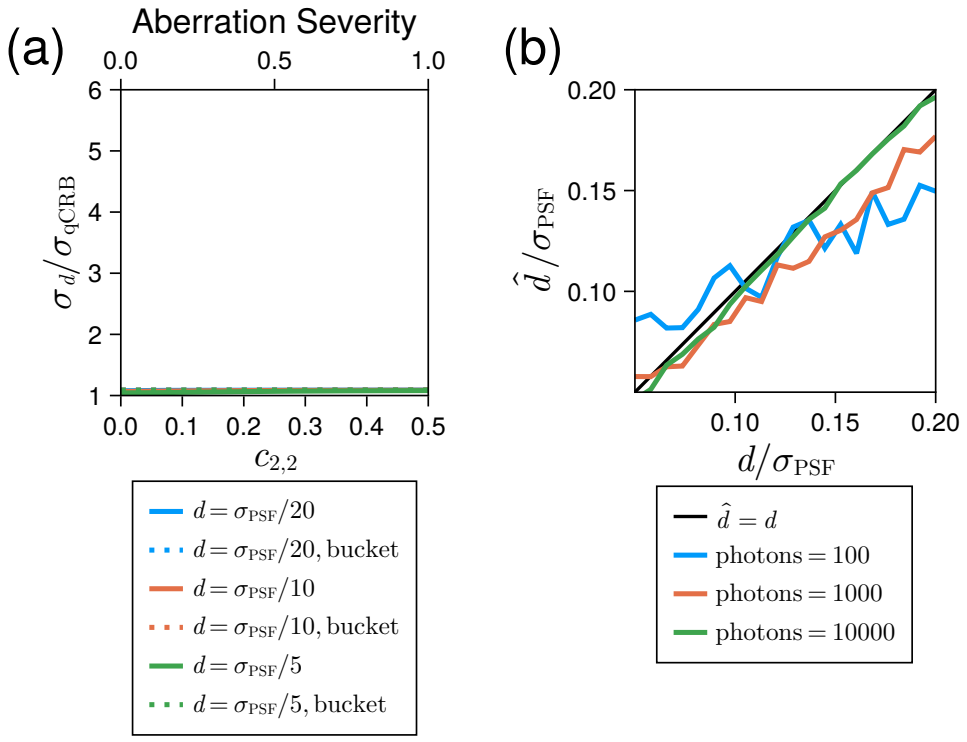

Fig. S9. Extra-SLIVER phase astigmatism. (a) $\sigma_d/\sigma_{\mathrm{qCRB}}$ as a function of increasing vertical astigmatism (n=2, l=2) at the interferometer entrance for pixelated (solid lines) and bucket (dashed lines) SLIVER measurements. (b) MLE of the separation for a Zernike coefficient of 0.25 at varying signal levels when the model has complete knowledge of the aberration.

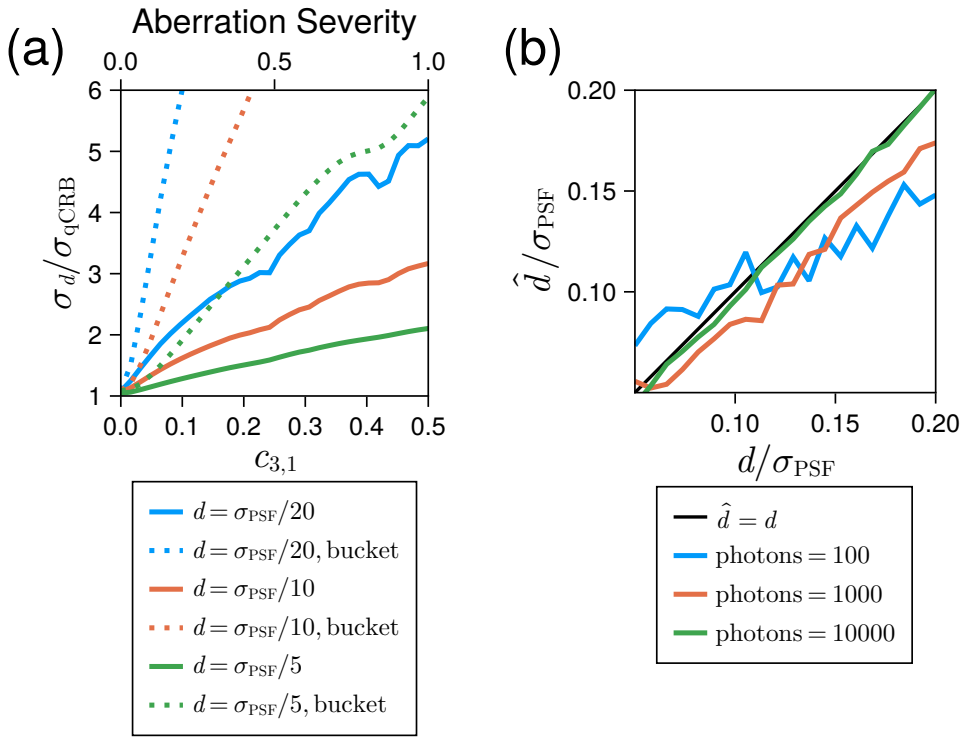

Fig. S10. Extra-SLIVER phase coma. (a) $\sigma_d/\sigma_{\mathrm{qCRB}}$ as a function of increasing horizontal coma (n=3, l=1) (i.e., coma along the axis of separation) at the interferometer entrance for pixelated (solid lines) and bucket (dashed lines) SLIVER measurements. (b) MLE of the separation for a Zernike coefficient of 0.25 at varying signal levels when the model has complete knowledge of the aberration.

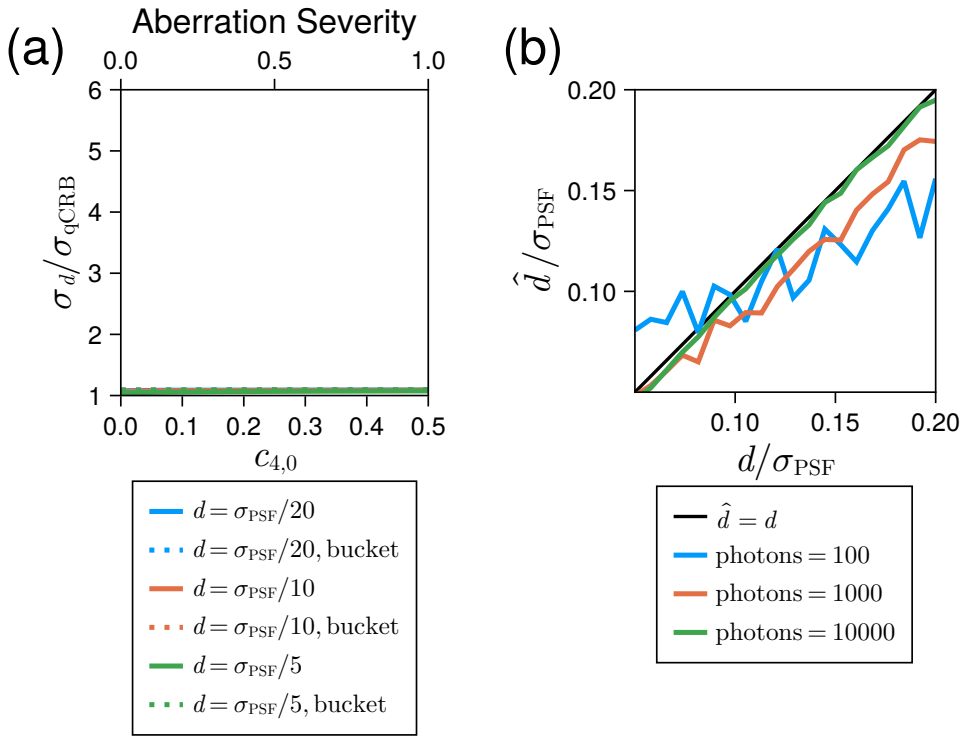

Fig. S11. Extra-SLIVER spherical phase aberration. (a) $\sigma_d/\sigma_{\mathrm{qCRB}}$ as a function of increasing spherical aberration (n=4, l=0) at the interferometer entrance for pixelated (solid lines) and bucket (dashed lines) SLIVER measurements. (b) MLE of the separation for a Zernike coefficient of 0.25 at varying signal levels when the model has complete knowledge of the aberration.

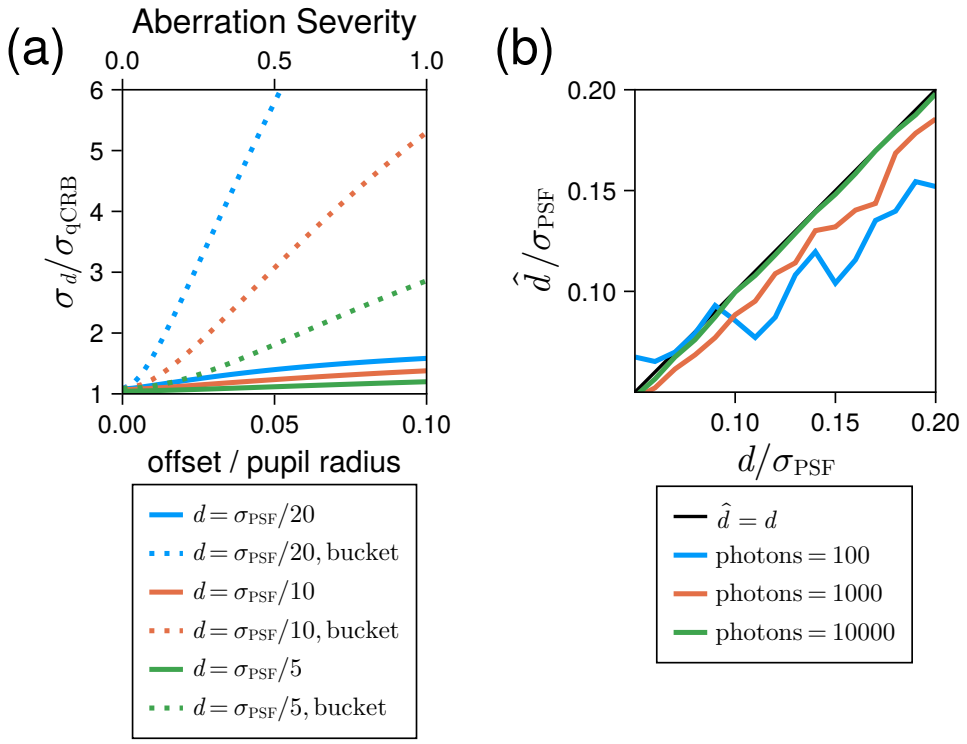

Fig. S12. Interferometer arm misalignment. (a) $\sigma_d/\sigma_{\mathrm{qCRB}}$ as a function of increasing interferometer arm misalignment for pixelated (solid lines) and bucket (dashed lines) SLIVER measurements. (b) MLE of the separation for a pupil offset of 0.05 times the pupil radius at varying signal levels when the model incorporates knowledge of the pupil offset.

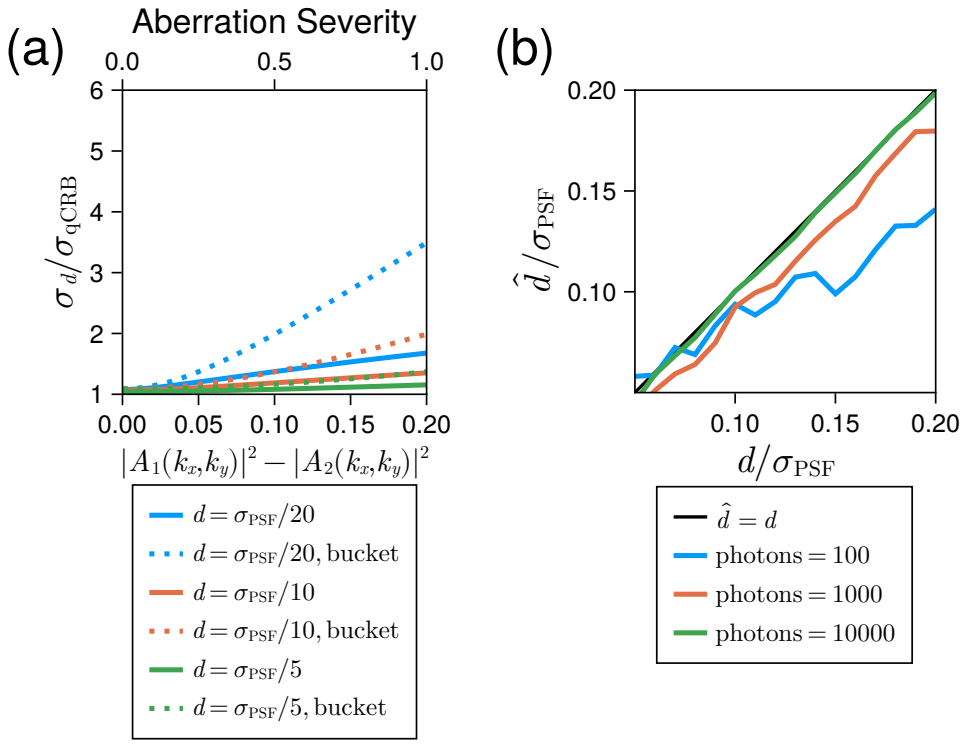

Fig. S13. Interferometer arm energy asymmetry. (a) $\sigma_d/\sigma_{\mathrm{qCRB}}$ as a function of increasing energy asymmetry between the interferometer arms for pixelated (solid lines) and bucket (dashed lines) SLIVER measurements. (b) MLE of the separation for an energy asymmetry $|A_2(k_x,k_y)|^2 - |A_1(k_x,k_y)|^2$ of 0.1 when the model incorporates knowledge of the asymmetry.

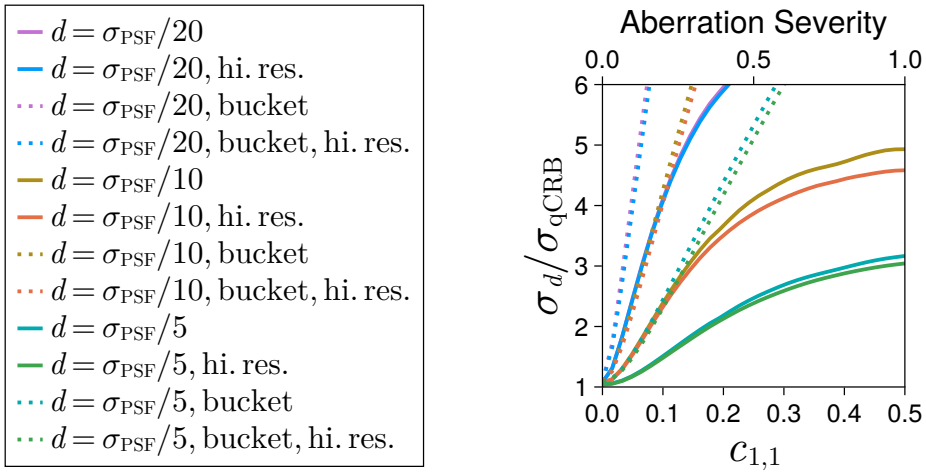

Fig. S14. Pixel size comparison. $\sigma_d/\sigma_{\mathrm{qCRB}}$ as a function of increasing horizontal tilt (n=1, l=1) in one arm of the interferometer for pixelated (solid lines) and bucket (dashed lines) SLIVER measurements and at differing pixel sizes. The lines indicated by "hi. res." were computed with a pixel size $\delta x' = \delta x/4$ where δx is the pixel size used to produce all other results shown in the manuscript.